

PAPER • OPEN ACCESS

Structure, hardness and fracture toughness of arc-melted $\text{LaB}_6\text{-TiB}_2$ eutectic alloy

To cite this article: D D Nesmelov *et al* 2019 *IOP Conf. Ser.: Mater. Sci. Eng.* **525** 012066

View the [article online](#) for updates and enhancements.



IOP | ebooks™

Bringing you innovative digital publishing with leading voices to create your essential collection of books in STEM research.

Start exploring the **collection** - **download the first chapter of every title for free.**

Structure, hardness and fracture toughness of arc-melted LaB₆-TiB₂ eutectic alloy

D D Nesmelov¹, S V Vikhman¹, E S Novoselov¹, S N Perevislov² and S S Ordan'yan¹

¹Saint-Petersburg State Institute of Technology, Saint-Petersburg, Russia

²Institute of Silicate Chemistry of Russian Academy of Sciences, Saint Petersburg, Russia

E-mail: dnesmelov@yandex.ru

Abstract. Microstructural and indentation-techniques mechanical investigations have been performed on a LaB₆-TiB₂ eutectic composite, obtained by the electric arc-melting in argon flow. Structure of solidified eutectics consists of directionally crystallized TiB₂ fibers in LaB₆ matrix. XRD, SEM and EDX analysis of eutectics were performed. The median diameter of the TiB₂ fibers, calculated using statistical analysis of SEM micrographs, was 0.45 μm. The volume fraction of the TiB₂ phase in eutectics was 16% as calculated by area fractions from SEM micrographs. The Vickers hardness (25.5 GPa) and fracture toughness (6.7 MPa·m^{1/2}) were measured on arc-melted LaB₆-TiB₂ alloy. Results were compared with the same ones, measured on floating-zone melted monocrystalline LaB₆.

1. Introduction

In addition to outstanding thermionic characteristics [1-3] and promising optical properties [4-7], lanthanum hexaboride exhibits high strength, hardness and Young's modulus. This fact is due to strong covalent bonds within the B₆ octahedron. One of the key characteristics of brittle materials, fracture-toughness, in case of LaB₆ single crystal is quite low - about 2.5-3.5 MPa·m^{1/2}. Near full-density polycrystalline LaB₆ demonstrates the same values of fracture-toughness. However, mechanical properties of LaB₆ can be enhanced by creating heterophase structures. It is possible on the base of LaB₆-MeB₂ systems (where Me = Ti, Zr, Hf, Cr, V, Nb etc.), all of them are eutectic [8]. As shown in [8-10], the creation of composite ceramic materials based on LaB₆-MeB₂ systems makes it possible to increase the fracture-toughness of the material to 3.7-4.5 MPa·m^{1/2}. This effect is associated with a more fine-grained structure of two-phase materials in comparison with single-phase ones due to the restriction of grain growth during sintering and a decrease in sintering temperature due to the presence of eutectic.

However, even more increase in mechanical properties can be achieved by creating a specific structure of directionally crystallized eutectics [11-17]. For example, Bogomol et al. described materials obtained by the floating-zone method, the crack resistance of which reaches 8.9 MPa·m^{1/2} [11]. In a number of other works, sufficiently high values of crack resistance in directionally crystallized eutectics in LaB₆-MeB₂ systems were also obtained [12-17].

In present study we investigated the microstructure, hardness and fracture-toughness of electric arc-melted LaB₆-TiB₂ eutectic composite. In contrast to floating-zone method, arc-melting does not allows to obtain unidirectional solidified alloy at macro-scale. The structure of arc-melted alloys can consist of differently oriented (according to different temperature gradients during crystallization) blocks of eutectics. It was of considerable interest to investigate the Vickers hardness and fracture-toughness of



arc-melted LaB₆-TiB₂ composite in comparison with the same characteristics of obtained by floating-zone method monocrystalline LaB₆.

2. Materials and Method

Commercial powders of LaB₆ (99.0 wt. %) and TiB₂ (99.0 wt. %) were used in this study. The average size of starting powders (the 50th percentile particle size, d_{50}) determined by laser diffraction was 12 and 15 μm respectively. Mixing combined with milling of powders was provided on vibratory ball-mill in gasoline-solvent media with TiB₂ balls (balls to material weight ratio B:M = 10:1) during 40 hours. Powders were mixed in eutectic concentration ratio 66 mol. % LaB₆ – 34 mol. % TiB₂ [8] with taking into account the additional 1.3 mass. % TiB₂, which appears at mixture due to the wear of TiB₂ balls. After the ball-milling the average size of mixture was $d_{50} = 3.5 \mu\text{m}$.

Vacuum-dried mixture was compacted into the tablets with diameter of 20 mm and height of 12 mm under the pressure of 1 t/cm² and then sintered at 1850 °C in vacuum of 10⁻² Pa during 1 hour.

Sintered tablets were put on a water-cooled cooper plate (anode) under argon gas flow and then electric arc-melted. After arc-melting and cooling of samples they were cut and polished for analysis.

Phase composition of alloy was determined using the X-ray diffraction (XRD) analysis (Rigaku SmartLab 3, Cu K α radiation, $\lambda = 1.5406 \text{ \AA}$) in the 2θ range of 10–90° with 0.01 ° step. Microstructure of alloy was investigated using optical microscope (Meiji 7000 with Thixomet-Lite system for image analysis) and SEM Tescan Vega 3SBH. For EDX analysis SEM was used with Aztec Energy Advanced analyzer (Oxford Instruments).

Indentation tests were carried out with use of Vickers hardness tester PMT-3 under the load of 7 to 13.2 N. Direction of indentations were so that the indenter diagonals were oriented perpendicular to the TiB₂ fibers. For calculation of Hv (Vickers hardness, GPa) we use equation (1):

$$Hv = 1,854 \cdot \frac{P}{D^2}, \quad (1),$$

where P – load, N; D – measured diagonal of the indentation, μm .

Fracture-toughness was K_{IC} calculated according to equation (2):

$$K_{IC} = 0,0889 \sqrt{\frac{Hv \cdot P}{4l}}, \quad (2)$$

where P – load, N; l – measured length of the crack from corner of indentation, μm .

At each load, at least 10 indentations were made, from which the mean values of the lengths of the diagonals and cracks was calculated.

3. Results and discussion

After the arc-melting the samples externally had the form of distorted ellipses with a matte surface with a metallic luster and a purple shade, inherent to lanthanum hexaboride. The lower part of the alloy, which was in contact with the copper substrate, was removed.

As can be clearly seen in the SEM images of cross-sectional arc-melted LaB₆-TiB₂ sample (Figure 1) the structure of crystallized objects is typically eutectic with the second phase (TiB₂) distributed in matrix (LaB₆). The distribution of the TiB₂ fibers (rods) is uniform, the individual eutectic blocks are separated by areas of crystallization of pure lanthanum hexaboride (Figure 1b). The median diameter of the TiB₂ fibers, calculated using statistical analysis of SEM micrographs of different fields of alloy, was 0.45 μm . The volume fraction of the TiB₂ phase in eutectics was 16% as calculated by area fractions from SEM micrographs, which is consistent with the literature data [8]. Weight Ti : La = 1 : 5.7 ratio determined by means of EDX also corresponded to the eutectic concentration of related borides.

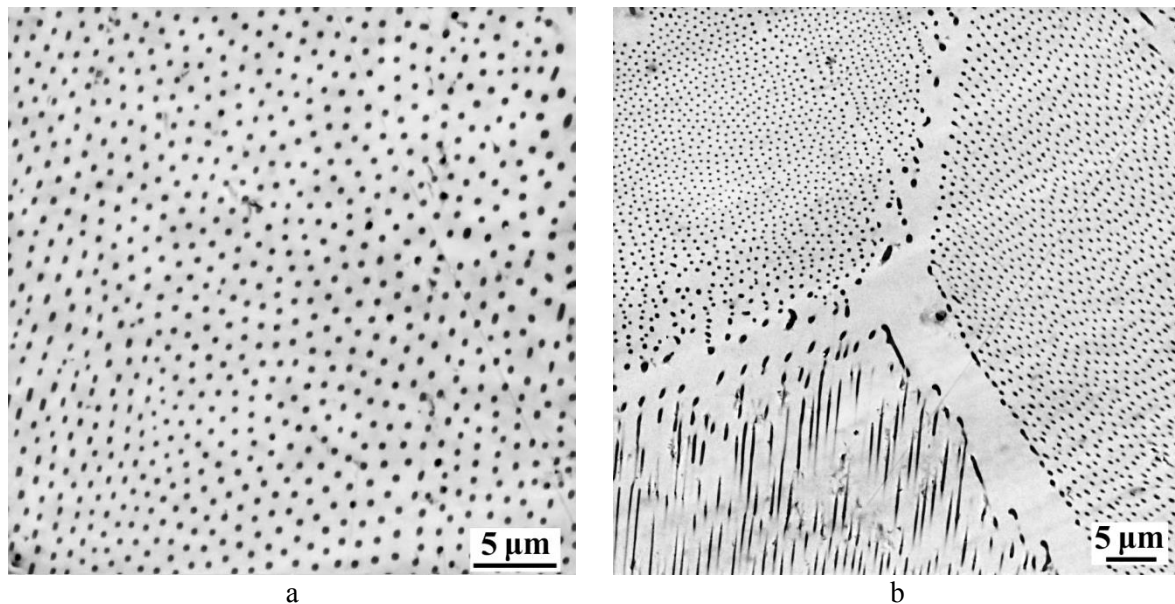


Figure 1. SEM images of cross-sectional arc-melted $\text{LaB}_6\text{-TiB}_2$ eutectic alloy

XRD-spectra of arc-melted alloy cross-section is presented at fig.2. In the spectra there are diffraction peaks of only two phases LaB_6 and TiB_2 . Almost threefold excess of the standard intensity of the LaB_6 [300] peak at $67.5623^\circ 2\theta$ indicates the fixation of a predominantly oriented structure.

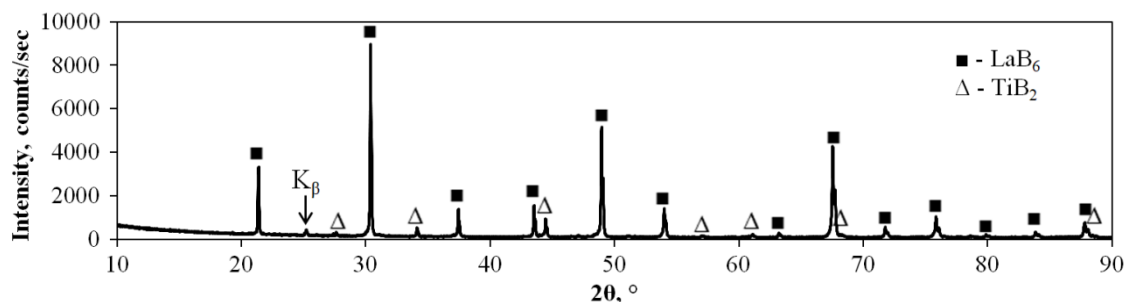


Figure 2. XRD patterns of arc-melted $\text{LaB}_6\text{-TiB}_2$ alloy cross-section

Mean hardness of $\text{LaB}_6\text{-TiB}_2$ alloy obtained by melting in electric arc ($H_v = 25.5$ GPa regardless of the load) was lower than the theoretical value calculated by the rule of mixtures (28.4 GPa). One of indentations is shown on fig. 3a. Hardness of single-crystalline LaB_6 (26 GPa) was correctly measured only at load of 7 N. Increasing the load led to the appearance of ring indentation-induced cracks and peeling of the material (Figure 3b), which did not allow to calculate the hardness and fracture-toughness of single crystal according to accepted methods. Unlike single-crystal, arc-melted alloy maintained without critical destruction all the loads applied to it, including 13.2 N. There no formation of ring cracks was observed.

Fracture toughness of $\text{LaB}_6\text{-TiB}_2$ alloy and LaB_6 single crystal was respectively 6.7 and 3.1 $\text{MPa}\cdot\text{m}^{1/2}$. High fracture-toughness values of arc-melted alloy are due to its “fiber self-reinforced” structure. Main mechanism of reinforcement in this case is due to an increase in the length of the crack propagation path because of its deflection by TiB_2 fibers, as it is shown on fig. 3c.

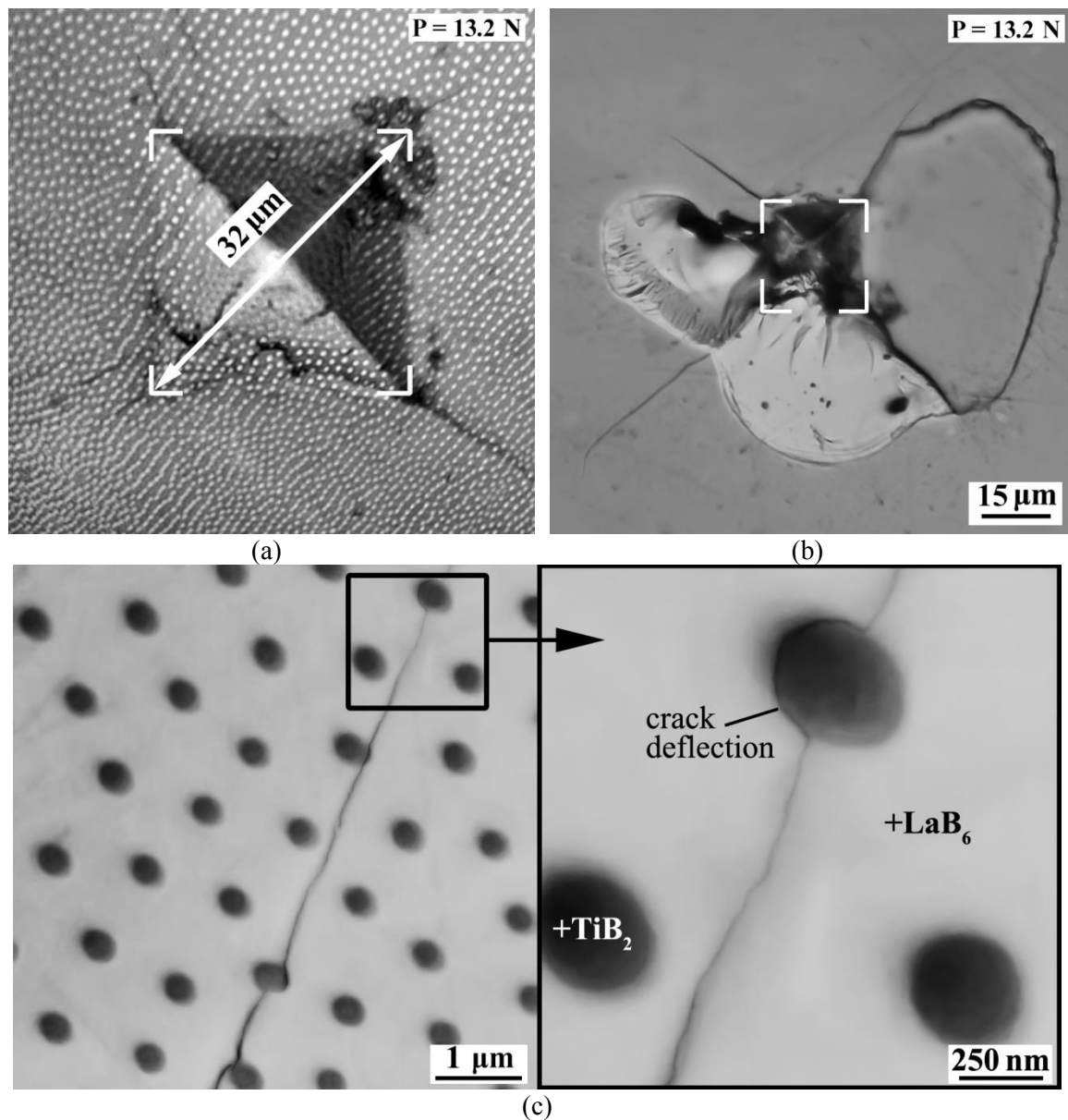


Figure 3. Optical images of Vickers indentations and indentation-induced cracks: **a** - arc-melted $\text{LaB}_6\text{-TiB}_2$ eutectics, **b** - single-crystalline LaB_6 , and **c** – SEM micrograph of crack deflection in arc-melted $\text{LaB}_6\text{-TiB}_2$ eutectics

4. Conclusion

Directionally-solidified $\text{LaB}_6\text{-TiB}_2$ eutectic alloy was obtained by the melting at electric arc in argon flow. Structure of eutectics consists of directionally crystallized TiB_2 fibers (rods) in LaB_6 matrix. The median diameter of the TiB_2 fibers was $0.45\ \mu\text{m}$, the volume fraction of the TiB_2 phase in eutectics was 16%. Arc-melted $\text{LaB}_6\text{-TiB}_2$ alloy demonstrated high values of Vickers hardness (25.5 GPa) and fracture toughness ($6.7\ \text{MPa}\cdot\text{m}^{1/2}$), which is due to mechanism of crack deflection by TiB_2 fibers.

Acknowledgments

The reported study was funded by RFBR project No 18-33-20221. Authors are grateful to the Engineering Centre of Saint-Petersburg State Institute of Technology for the equipment provided.

References

- [1] Lafferty J M 1951 *Journal of Applied Physics* **3** 299
- [2] Taran A, Voronovich D, Oranskaya D, Filipov V, Podshyvalova O 2013 *Functional materials* **4** 485
- [3] Paderno Y B, Taran A A, Voronovich D A, Paderno V N, Filipov V B 2008 *Functional materials* **1** 63
- [4] Kowalczyk J M, Hadmack M R, Szarmes E B, Madey J M 2014 *International Journal of Thermophysics* **8** 1538
- [5] Mattox T M, Coffman D K, Roh I, Sims C, Urban J J 2018 *Materials* **2** 226
- [6] Mattox T, Urban J 2018 *Materials* **12** 2473
- [7] Sani E, Mercatelli L, Meucci M, Zoli L, Sciti D 2017 *Scientific Reports* **1** 718
- [8] Ordanyan S S, Vikhman S V, Nesmelov D D, Danilovich D P, Panteleev I B 2014 *Advances in Science & Technology* **89** 47.
- [9] Min G H, Gao R, Yu H S, Han J 2005 *Key Engineering Materials* **297** 1630
- [10] Wang X., Zhang J X, Yang X Y, Hu K, Zhang J W 2017 *Advances in Applied Ceramics* **3** 132
- [11] Bogomol I, Nishimura T, Nesterenko Y, Vasylykiv O, Sakka Y, Loboda P 2011 *Journal of Alloys and Compounds* **20** 6123
- [12] Soloviova T O, Karasevska O P, Vleugels J, Loboda P I 2017 *Journal of Alloys and Compounds* **729** 749
- [13] Chen C M, Zhang L T, Zhou W C 1998 *Journal of crystal growth* **4** 873
- [14] Yang X, Wang P, Wang Z, Hu K, Cheng H, Li Z, Zhang J 2017 *Materials & Design* **133** 299
- [15] Volkova H, Filipov V, Podrezov Y. 2014 *Journal of the European Ceramic Society* **14** 3399
- [16] Jouanny I, Sennour M, Berger M H, Filipov V B, Ievdokymova A, Paderno V N, Sayir A 2014 *Journal of the European Ceramic Society* **9** 2101
- [17] Loboda P I, Soloviova T O, Bogomol Y I, Remizov D O, Bilyi O I 2015 *Journal of Superhard Materials* **6** 394